Aachen Institute for Advanced Study in Computational Engineering Science

Preprint: AICES-2010/07-1

1/July/2010

Phase-Field Modeling of Elastic Effects in Eutectic Growth with Misfit Stresses

Z. Ebrahimi, J. L. Rezende, J. Kundin

RWTH AACHEN UNIVERSITY

AI CES

Financial support from the Deutsche Forschungsgemeinschaft (German Research Association) through grant GSC 111 is gratefully acknowledged.

List of AICES technical reports: http://www.aices.rwth-aachen.de/preprints

Phase-Field Modeling of Elastic Effects in Eutectic Growth with Misfit Stresses

Z. Ebrahimi[1], J. L. Rezende[2], J. Kundin[2]

1. AICES Graduate School, RWTH Aachen University, D-52056 Germany
2. Institute of Minerals Engineering (GHI), RWTH Aachen University, D-52056 Germany

Abstract

Elastic interactions, arising from a difference of lattice spacing between two coherent phases in eutectic alloys with misfit stresses, can have an influence on microstructural pattern formation of eutectic colonies during solidification process. From a thermodynamic point of view the elastic energy contributes to the free energy of the phases and modifies their mutual stability. Therefore, the elastic stresses will have an effect on stability of lamellae, lamellae spacing and growth modes. In this paper, a phase-field model is employed to investigate the influence of elastic misfits in eutectic growth. The model reduces to the traditional sharp-interface model in a thin-interface limit, where the microscopic interface width is small but finite. An elastic model is designed, based on linear microelasticity theory, to incorporate the elastic energy in the phase-field model. Theoretical and numerical approaches, required to model elastic effects, are formulated and the stress distributions in eutectic solidification structures are evaluated. The two dimensional simulations are performed for directed eutectic growth and the simulation results for different values of the misfit stresses are illustrated.

1 Introduction

Numerous experiments and numerical studies have attempted to investigate the microstructural evolution in binary alloys and eutectic structures [1, 2, 3] including eutectic front behavior as the interface undergoes various instabilities and exhibits some nonlinear features such as bifurcations [4, 5, 6, 7, 8]. In eutectic solidification two or more phases grow simultaneously from the liquid in a coupled manner and can exhibit a wide variety of geometrical arrangements [9].

The phase-field approach has been employed widely to predict the phase transition and solidification process in multicomponent and multiphase systems [10, 11, 12]. It is a genuine representation of the original free-boundary problem (FBP) in sharp-interface limit as the interface thickness tends to zero. In the phase-field concept the interfacial boundary conditions are avoided by introducing a set of smooth variables, the so-called phase-field variables, which characterize time and spacial evolutions of bulk phases in the underlying system. In the past decay several models for eutectic growth have been developed. In the diffusion limited eutectic growth the phase and concentration fields are evolved by chemical driving forces accommodated by chemical free energies [13, 15, 14]. However there are several additional phenomena that influences the phase transformations in alloys including elastic interactions arising from a difference of lattice spacing between two coherent phases, grain boundary diffusion and concentration dependent diffusion coefficients [16, 17, 18].

Experimental observations in some alloy systems show that to reveal the solidification behaviour of a group of eutectic alloys, the influence of the misfit strain occurring on the interface between two growing phases of different lattice parameters should be considered [19, 20]. In other words, the elastic energy contributes to the free energy of the phases and alter the morphology of the phases inside the eutectic structures. The inclusion of the misfit stress requires additional differential equations for describing the elastic deformation as well as the coupling of the mechanical dynamics to the phase-field evolution equation. At this point the resulting energy contribution should be treated as an interface energy in the phase-field ansatz. This model differs from the usual models for phase transformations including elastic energy, like those by Khachaturyan [21], since the microstructure is formed by solidification processes instead of phase transitions in solids as it is the case for i.e. martensitic transformation [22].

We have developed a phase-field model based on linear microelasticity theory, which is capable to incorporate elastic energy and coherent elastic misfit to eutectic growth. The driving force of the system is arising from the misfit between two different solid phases as well as the gradient of the diffusion potential for solute diffusion. A smooth free-enrgy function is defined with assumption that in the boundary between two phases no third phase is present. It consists of a chemical free-energy based on previous models for multi-phase and two-phase growth [14, 15] and an elastic part that accommodates the misfit stress between eutectic lamellae. The governing equations that describe the coupling relations among phase-field variables, concentration and stress/strain fields include the phase-fields equations, the diffusion equation and mechanical equilibrium to evaluate the elastic displacements. In Sec. 2 we present our phase-field model for a three phase system. The elastic, interfacial and chemical free-energies are defined and system evolutionary equations are derived by applying a variational formulation. The equation for the mechanical equilibrium is governed in Sec. 2.4 for a class of binary alloys that involves a single liquid and two solid phases, which are considered here. We show that on each solid-liquid interface the model reduces to the standard model of single phase solidification (Sec. 2.5). Sec. 3 is devoted to the numerical simulations. The directional solidification , in which the samples are pulled from a hot into a cold region with a constant velocity, have been used as a relevant example to study the lamellar growth in binary alloys [24, 25]. The microstructure formed in this situation, the so-called two-phase growth, consist of the lamellae of different solid phases with a front spacing λ. We use this as a test ground for our model in Sec. 3.2. Finally major results are summarized in Sec. 4.

2 Phase-Field Model

In this section we develop the phase-field model for eutectic growth. First we introduce a free energy for the system as in the standard phase-field model, Sec. 2.1, and define its elastic part in Sec. 2.2. Next we derive the system eqution of motion by using the general variational formulation (Sec. 2.3). At the end, the reduction to single phase solidification is captured in Sec. 2.5.

2.1 Free Energy Function

We define a set of continues scalar variables, the so-called phase-field variables, as a volume fraction of phase i. Each phase-field variable is unity in the corresponding i-th single phase

region and zero outside that phase, i.e $p_i \in [0,1]$, and should satisfy

$$\sum_i p_i = 1, \tag{1}$$

where $i = \alpha, \beta, L$ represents two solid and a liquid phase. The material system is described by the volume integral of a free energy density

$$F = \int_V f dV. \tag{2}$$

The dimensionless free energy density is the sum of the interfacial free energy, the chemical free energy and the elastic free energy,

$$f(\vec{p}, c, T) = \frac{K}{2}(\vec{\nabla}\vec{p})^2 + H f_p(p_i) + X f_{ch}(\vec{p}, c, T) + Y f_{el}(\vec{p}, \vec{u}). \tag{3}$$

The first term on rhs of Eq. (3) is the kinetic part of the interface energy. The dimensionless functions f_p, f_{ch} and f_{el} must have three local minimum to account for three possible phases, i.e α, β and the liquid phase. f_p is the potential part of the interfacial energy. We define f_p as the sum of double-well potentials

$$f_p = \sum_i p_i^2 (1 - p_i)^2. \tag{4}$$

The chemical free energy density, f_{ch}, defines the equilibrium phase-diagram of the system and sets the chemical driving forces. The constants H, X and Y have the dimension of energy per volume and K has the dimension of energy per unit length. Several phase-filed models that deduce the chemical free energy density from thermodynamical databases have been reported [13, 15, 24]. Here we formulate $f_{ch}(c, T)$ as the mixture free energy density, where c is the mixture concentration and T is the temperature. Assume $A_i(T)$ is the concentration of a phase i in equilibrium with phase j and B_i is the free energy density of individual phases $f_{ch,i}(A_i, T)$ in equilibrium. With this notation the chemical free energy density of phases can be written as [14]

$$f_{ch,i}(c, T) = (c - A_i(T))^2/2 + B_i(T) \tag{5}$$

and for the mixture chemical free energy density we get

$$f_{ch}(\vec{p}, c, T) = \frac{1}{2}(c - \sum_i A_i(T) g_i(\vec{p}))^2 + \sum_i B_i(T) g_i(\vec{p}), \tag{6}$$

where the mixture equilibrium parameters are waighted by the functions g_i. We choose the functions g_i by analogy with Ref. [14] as

$$g_i = \frac{p_i^2}{4}\left(15(1 - p_i)[1 + p_i - (p_k - p_j)^2] + p_i(9p_i^2 - 5)\right). \tag{7}$$

The mixture diffusion potential μ is defined as

$$\mu = \frac{1}{X}\frac{\delta F}{\delta c} = \frac{\partial f_{ch}}{\partial c} = c - \sum_i A_i(T) g_i(\vec{p}). \tag{8}$$

One should distinguish the diffusion potential from the thermodynamically defined chemical potential.

2.2 Elastic Free Energy

The last term in Eq. (3), $f_{el}(\vec{p},\vec{u})$, is the contribution due to lattice misfit between solid phases in the eutectic system, where $\vec{u}$ is the displacement field. We employ the isotropic linear elasticity and assume elastic inhomogeneities to evaluate stress and strain tensors

$$\sigma_{ij} = (2\mu\epsilon_{ij} + \lambda\epsilon_{kk}\delta_{ij}), \tag{9}$$

$$\epsilon_{ij} = \frac{1}{2}\left(\frac{\partial u_i}{\partial x_j} + \frac{\partial u_j}{\partial x_i}\right), \tag{10}$$

where λ and μ are Lame constants and i, j denote the spacial coordinates. Do not confuse with diffusion potential and a lamellae spacing (see below). To incorporate the influence of the misfit between lamellae of different phases we introduce the misfit strain ϵ_m which accommodates the misfit stress σ^m_{ij} on the boundary between two solid phases, α and β.

$$\sigma^m_{ij} = -\xi\delta_{ij} \tag{11}$$

with

$$\xi = \epsilon_m(2\mu + d\lambda) \tag{12}$$

where d is the dimension of the underlying system. The stress tensor in individual phases with different Lame coefficients λ^s and μ^s can be modified to include the misfit term on the interface,

$$\sigma^s_{ij} = (2\mu^s\epsilon_{ij} + \lambda^s\epsilon_{kk}\delta_{ij}) - \xi^s\delta_{ij} \quad \text{for } s = \alpha, \beta. \tag{13}$$

In general the elastic energy in a continuum system is

$$F_{el} = \int_V Y f_{el} dV = \frac{1}{2}\int_V \sigma_{ij}\epsilon_{ij} dV. \tag{14}$$

The phase dependent elastic free energy density of the system can be constructed by the sum of the elastic free energy densities of individual phases f^s_{el} weighted by function $h(p_s)$ that should satisfy $h(p_i = 1) = 1$, $h(p_i = 0) = 0$ and $h'(p_i = 0, 1) = 0$, analogous to Ref. [23]

$$f_{el} = \sum_{s=\alpha,\beta} h(p_s) f^s_{el}, \tag{15}$$

the same relation holds for σ_{ij}

$$\sigma_{ij} = \sum_{s=\alpha,\beta} h(p_s)\sigma^s_{ij}. \tag{16}$$

Denote that we have assumed zero elastic fields in the liquid in our formulations. Using the definition of the stress tensor from Eqs. (12), (13) and (14) we get

$$f^s_{el} = \frac{1}{Y}\left[\mu^s(\epsilon_{ij} - \epsilon^m\delta_{ij})^2 + \frac{\lambda^s}{2}(\epsilon_{kk} - d\epsilon^m\delta_{ij})^2\right]. \tag{17}$$

The elastic free energy densities of individual phases are reduced in 2D case to

$$\begin{aligned} f^s_{el} \;=\; & \frac{1}{Y}[\mu^s(\epsilon^2_{xx} + \epsilon^2_{yy} + 2\epsilon^2_{xy}) + \frac{\lambda^s}{2}(\epsilon_{xx} + \epsilon_{yy})^2 + \\ & (\mu^s + \lambda^s)\epsilon^2_m - 2(\mu^s + \lambda^s)\epsilon_m(\epsilon_{xx} + \epsilon_{yy})]. \end{aligned} \tag{18}$$

2.3 Evolutionary Equations

The equations of motion for the phase-field variables are derived by minimization of the free energy functional F. The spatial-temporal evolution of phase-field variables defines the growth of an arbitrary microstructure. In this context two coupled non-linear partial differential equations describe the evolution of the interface and the equilibrium front problem.

$$\tau(p_i)\frac{\partial p_i}{\partial t} = -\frac{1}{H}\frac{\delta F}{\delta p_i}|_{\sum_i p_i=1} \quad \forall i, \tag{19}$$

where $\tau(p_i)$ is a relaxation time. While evaluating the functional derivative, we should consider the constrain $\sum_i p_i = 1$ and assume that on the interface $i-j$, connecting two phases i and j, no other phase is present, i.e $p_k = 0, k \neq i, j$ [14]. This means that in triple point the transition between the phases occurs by the movement of the dual boundaries that do not influence each other.

The temporal evolution of the concentration c is described by the diffusion equation

$$\frac{\partial c}{\partial t} = \vec{\nabla} \cdot \left(M(\vec{p})\vec{\nabla}\frac{\delta F}{\delta c} \right), \tag{20}$$

where $M(\vec{p})$ is the chemical mobility. Substituting the chemical potential given by Eq. (8) in Eq. (20) the continuity equation becomes,

$$\frac{\partial \mu}{\partial t} = \vec{\nabla} \cdot \left(D(\vec{p})\vec{\nabla}\mu - \vec{j}_{at} \right) - \sum_i A_i \frac{\partial g_i(\vec{p})}{\partial t} \quad \forall i, \tag{21}$$

where $D(\vec{p}) = \sum_j D_j p_j$ and D_j represents the diffusion coefficient of the phase j. In the phase-field simulation we use an interface thickness, which is larger than the experimental length scale, to model the interfacial growth in real materials. When the diffusion is asymmetrical the solute trapping occurs at the interface in this situation [24]. These non-equilibrium effects become important when we define the diffusion coefficient in Eq. 21 as $D(\vec{p}) = Dp_L$, where p_L is the volume fraction of the liquid phase. This means that the solute diffusity varies from zero in the solid to D in the liquid. Therefore the effects of solute trapping should be eliminated by adding the anti-trapping current $\vec{j}_{at}$ to the diffusion equation, which for a two-phase system can be obtained as

$$\vec{j}_{at} = -aW\vec{n}_L \sum_{i=\alpha,\beta} (A_L - A_i)(\vec{n}_L \cdot \vec{n}_i)\frac{\partial p_i}{\partial t} \tag{22}$$

with $a = 1/\sqrt{2}$ (See Ref. [14, 24] for the details). The derivative $\delta F/\delta p_i|_{\sum_i p_i=1}$ in Eq. (19) can be evaluated by the method of Lagrange multipliers analogous to [14]. Using this the evolution equation reads

$$\begin{aligned} \tau(p_i)\frac{\partial p_i}{\partial t} &= W^2\nabla^2 p_i - \frac{\partial f_p}{\partial p_i} - \frac{1}{3}\sum_j \frac{\partial f_p}{\partial p_j} \\ &-\lambda_c\left(\frac{\partial f_{ch}}{\partial p_i} - \frac{1}{3}\sum_j \frac{\partial f_{ch}}{\partial p_j}\right) - \lambda_e\left(\frac{\partial f_{el}}{\partial p_i} - \frac{1}{3}\sum_j \frac{\partial f_{el}}{\partial p_j}\right), \end{aligned} \tag{23}$$

where the variations are taken as if all p_i were independent. The parameters W, λ_c and λ_e are defined by comparing Eq. (19) with Eq. (3)

$$W = \sqrt{\frac{K}{H}}, \quad \lambda_c = \frac{X}{H}, \quad \lambda_e = \frac{Y}{H}. \tag{24}$$

Replacing the components of the free energy density, f_p (Eq. 4), f_{ch} (Eq. 6) and f_{el} (Eq. 15) in Eq. (19) we obtain

$$\tau(p_i)\frac{\partial p_i}{\partial t} = W^2\nabla^2 p_i + \frac{2}{3}[-2p_i(1-p_i)(1-2p_i) + \sum_{j\neq i} p_j(1-p_j)(1-2p_j)] + \lambda_c \sum_j \frac{\partial g_j}{\partial p_i}|_{\sum_i p_i=1} (\mu A_j - B_j) - \lambda_e \sum_j \frac{\partial h_j}{\partial p_i}|_{\sum_i p_i=1} f_{el}^j \quad \forall i. \tag{25}$$

2.4 Mechanical Equilibrium

The evolutionary equations (Eq. 25) should be solved together with equations for the evolution of the elastic variables. One should note that strain values ϵ_{ij} $(i,j=1,...d)$, depend on displacements $u_i(i=1,...d)$ trough (10), where i,j are the spacial coordinates. Assuming that mechanical equilibrium is always maintained within the system, one readily obtains a set of nonlinear equations.

$$\frac{\delta F_{el}}{\delta u_i} = \frac{\partial}{\partial x_j}\frac{\delta F_{el}}{\delta \epsilon_{ij}} = 0 \tag{26}$$

which means that at equilibrium condition, the variational derivatives $\delta F_{el}/\delta u_i$ of the elastic free energy is assumed to be zero. Substituting for F_{el} from equation (14) and (16) results in,

$$\frac{\partial}{\partial x_j}\left(\sum_s \tilde{h}(p_s)\sigma_{ij}^s\right) \text{ for } s=\alpha,\beta, \tag{27}$$

where we use a modified waighting function to exclude the liquid phase:

$$\tilde{h}(p_s) = \frac{h(p_s)}{\sum_{s=\alpha,\beta} h(p_s)}. \tag{28}$$

Employing Eq. (13) for stress tensor and replacing strains ϵ_{ij} with displacements, Eq. (10), we obtain a system of differential equations that needs to be solved with appropriate boundary conditions to find the displacements u_i. Once the displacements are found, the strain and stress tensor values can be obtained using the corresponding expressions.

For two phase growth the equilibrium requirements (27) reduces to the following equation,

$$\frac{\partial}{\partial x_j}\left(\tilde{h}(p_\alpha)\sigma_{ij}^\alpha + \tilde{h}(p_\beta)\sigma_{ij}^\beta\right) = \frac{\partial\tilde{h}(p_\alpha)}{\partial x_j}\sigma_{ij}^\alpha + \tilde{h}(p_\alpha)\frac{\partial\sigma_{ij}^\alpha}{\partial x_j} + \frac{\partial\tilde{h}(p_\beta)}{\partial x_j}\sigma_{ij}^\beta + \tilde{h}(p_\beta)\frac{\partial\sigma_{ij}^\beta}{\partial x_j} = 0. \tag{29}$$

A two dimensional model where x and y are the spacial coordinates is considered here. In this case the displacement vector $\vec{u}$, the stress and strain tensors can be expressed as,

$$\vec{u} = \begin{pmatrix} u_x & u_y \end{pmatrix}$$

$$\vec{\sigma} = \begin{pmatrix} \sigma_{xx} \\ \sigma_{yy} \\ 2\sigma_{xy} \end{pmatrix}$$

$$\vec{\epsilon} = \begin{pmatrix} \epsilon_{xx} \\ \epsilon_{yy} \\ 2\epsilon_{xy} \end{pmatrix}.$$

We now expand Eq. (29) for $i, j = x, y$ and substitute σ_{ij} and ϵ_{ij} from Eq. (13) and (10), respectively. Consequently, we obtain a system of two differential equations in terms of the displacement fields u_x and u_y

$$\begin{aligned} &\lambda(\frac{\partial^2 u_x}{\partial x^2} + \frac{\partial^2 u_y}{\partial y \partial x}) + 2\mu \frac{\partial^2 u_x}{\partial x^2} + \mu(\frac{\partial^2 u_x}{\partial y^2} + \frac{\partial^2 u_y}{\partial x \partial y}) \\ &+ \sum_{s=\alpha,\beta} [\lambda^s(\frac{\partial u_x}{\partial x} + \frac{\partial u_y}{\partial y}) + 2\mu^s \frac{\partial u_x}{\partial x} - \xi^s) \frac{\partial \tilde{h}(p_s)}{\partial x} \\ &+ \mu^s(\frac{\partial u_x}{\partial y} + \frac{\partial u_y}{\partial x}) \frac{\partial \tilde{h}(p_s)}{\partial y}] = 0 \end{aligned} \tag{30}$$

$$\begin{aligned} &\lambda(\frac{\partial^2 u_y}{\partial y^2} + \frac{\partial^2 u_x}{\partial x \partial y}) + 2\mu \frac{\partial^2 u_y}{\partial y^2} + \mu(\frac{\partial^2 u_y}{\partial x^2} + \frac{\partial^2 u_x}{\partial y \partial x}) \\ &+ \sum_{s=\alpha,\beta} [\lambda^s(\frac{\partial u_x}{\partial x} + \frac{\partial u_y}{\partial y}) + 2\mu^s \frac{\partial u_y}{\partial y} - \xi^s) \frac{\partial \tilde{h}(p_s)}{\partial y} \\ &+ \mu^s(\frac{\partial u_x}{\partial y} + \frac{\partial u_y}{\partial x}) \frac{\partial \tilde{h}(p_s)}{\partial x}] = 0, \end{aligned} \tag{31}$$

where

$$\mu = \sum_{s=\alpha,\beta} \tilde{h}(p_s)\mu^s$$

$$\lambda = \sum_{s=\alpha,\beta} \tilde{h}(p_s)\lambda^s$$

and

$$\xi^s = \mp \frac{\epsilon_m}{2}(2\lambda^s + 2\mu^s) \text{ for } s = \alpha(-), \beta(+).$$

The elasticity equations are only space dependent and therefore they can be solved independently of the phase-filed and concentration evolution equations. Once the displacements are found, the corresponding strains will be computed from linear elasticity formulations, Eq. (10). After that the calculated component of the strain tensor will be substituted in the phase-filed evolution equation and the phase-filed variable will be evaluated at each time step.

2.5 Mapping of the model to single-phase solidification

In the evolution equation, Eq. (25), there are two terms responsible for the driving force: the chemical term and the elasticity term. To mapping the present model with elastic effects to the single-phase solidification model we transform the Eq. (25) to a form with the chemical driving force as a leading force for the solidification, which is offset by the elastic effects.

The evolution equation can be rewritten with an assumption $h(\vec{p}) = g(\vec{p})$ and $\lambda_c = \lambda_e$ (that means $X = Y$ according to Eq. (24)) in the following form:

$$\tau(\vec{p})\frac{\partial p_i}{\partial t} = W^2\nabla^2 p_i + f_{p,p}(\vec{p}) + \lambda_c \sum_j \frac{\partial g_j}{\partial p_i}|_{\sum_i p_i=1}\left(\mu A_j^* - B_j^*\right), \tag{32}$$

where $f_{p,p}(\vec{p})$ is the derivative of the doable well function written in Eq. (23) and

$$\mu A_j^* - B_j^* = \mu A_j - B_j - f_{el}^j \tag{33}$$

is a transformed driving force for the solidification.

Now we show that for each solid-liquid interface this transformed evolution equation in the case of elastic effects can be mapped to single-phase solidification, similar to the derivation presented in the work of Folch and Plapp [14]. For two phases (liquid L and solid i) the evolution equation is simplified to

$$\tau_i\frac{\partial p_i}{\partial t} = W^2\nabla^2 p_i + f_{p,p}(p_i) + \lambda_c\frac{\partial g_i}{\partial p_i}\left(A_L^* - A_i^*\right)^2 u, \tag{34}$$

where we choose a dimensionless variable

$$u = \frac{\left(\mu - \mu_{eq}^{Li^*}\right)}{\left(A_L^* - A_i^*\right)} \tag{35}$$

with

$$\mu_{eq}^{Li^*} = \frac{B_L^* - B_i^*}{A_L^* - A_i^*} \tag{36}$$

being an equilibrium chemical potential between solid and liquid phases in the presence of an elastic field. The corresponding diffusion equation is

$$\frac{\partial u}{\partial t} = \vec{\nabla}\cdot\left[D(\vec{p})\vec{\nabla}u\right] + \frac{\partial g_i}{\partial t}. \tag{37}$$

With a constant relaxation time and a constant diffusivity this equations correspond to the phase-field model for the solidification of a pure substance for which the thin interface analysis treated by Karma and Rappel [26] can be applied.

To evaluate the unknown equilibrium parameters A_i^* and B_i^* the following considerations can be used. The diffusion resolved by means of Eq. (37) should not depend on the elastic effects to satisfy the standard model of solidification of a pure substance, so that the variable u should not change. This assumption leads to the relation

$$\frac{\left(\mu - \mu_{eq}^{Li^*}\right)}{\left(A_L^* - A_i^*\right)} = \frac{\left(\mu - \mu_{eq}^{Li}\right)}{\left(A_L - A_i\right)}, \tag{38}$$

where we assume $A_L^* = A_L = 0$ and $B_L^* = B_L = 0$ similar to [14], because in the liquid phase there are no elastic effects. The solution of Eq. (38) together with Eq. (33) for values A_i^* and B_i^* gives

$$A_i^* = A_i\sqrt{1 - \Delta_{el}^i} \tag{39}$$

and

$$B_i^* = B_i\left(1 - \Delta_{el}^i\right) - \mu A_i\left(1 - \Delta_{el}^i - \sqrt{1 - \Delta_{el}^i}\right), \tag{40}$$

where

$$\Delta^i_{el} = \frac{f^i_{el}}{(\mu A_i - B_i)} \tag{41}$$

is a dimensionless term, responsible for the elastic effects, that must be greater than 1.

According to the thin-interface limit analysis and the Gibbs-Thompson boundary condition [14, 26] the following relations for the kinetic coefficients have to be satisfied:

$$\lambda_c = \frac{a_1 W}{2\bar{d}} \left(\frac{1}{|A^*_\alpha|} + \frac{1}{|A^*_\beta|} \right) \tag{42}$$

and for the case without kinetic effects,

$$\tau_i = \frac{a_2 \lambda_c W^2 A_i^2}{D} \left(1 - \Delta^i_{el} \right) \tag{43}$$

with $i = \alpha, \beta$ for the two solid phases; $\bar{d} = (d_\alpha + d_\beta)/2$ is the mean capillary length; and a_1 and a_2 are the numerical constants. For the standard choice of the functions $f_p(\vec{p})$ and $g(\vec{p})$ $a_1 = \sqrt{2}/3$ and $a_2 = 0.7464$.

It can be see from Eq. (43) that the kinetic coefficients of a phase transition are not constants and should depend on the position of the interface in correspondence to the distribution of elastic fields. Moreover, after tdividing the evolution eaustion (34) by τ_i the interfacial terms have to increase with increasing elastic energy.

3 Simulations of Eutectic Growth

3.1 Model Parameters

We simulate the directional solidification of the transparent organic eutectic alloy $CBr_4 - C_2Cl_6$ whose properties are available in literature. The material parameters and process control parameters such as pulling velocity v_p and thermal gradient G, are listed in Table 1. In this system three phases, α, β and liquid phase, grow along the $y-$direction, while the sample is pulling back with velocity v_p. Temperature at a given point is

$$T = T_E + G(y - v_p t) \tag{44}$$

where T_E is the eutectic temperature. One can see from Table 1 that the mean capillary length $\bar{d}$ is several orders of magnitude larger than the thermal length $\bar{l}_T$, and the diffusion length, $l_D = D/v_p$. $\bar{l}_T$ is the average value of thermal length of each individual phase l^i_T,

$$l^i_T = |m_i| \triangle C/G \quad i = \alpha, \beta, \tag{45}$$

where $\triangle C = C_\alpha - C_\beta$; C_α and C_β are the compositions of α and β phases at T_E. As in the standard phase-field models [26] the interface thickness W should be larger than $\bar{d}$ to make the phase-field simulations feasible. Therefore we choose $W/\bar{d}$ as the resolution for our model in a way to fulfill the above requirement. The ratios $\bar{l}_T/l_D$ and $\lambda/\bar{d}$, where λ is the lamellar spacing fixed by the lateral size of simulation box, are also taken as input in the model. The coupling constant ,λ_c, and the time relaxation of each individual phase $\tau_i, i = \alpha, \beta$, are given in Eq. (42) and (43). We define the phase dependent relaxation time as

$$\tau(\vec{p}) = \bar{\tau} + \frac{\tau_\beta - \tau_\alpha}{2} \left(\frac{p_\beta - p_\alpha}{p_\alpha + p_\beta} \right), \tag{46}$$

Table 1: Materials parameters for a symmetric eutectic alloy used in the phase-field simulations and the corresponding length scales for directional solidification [14]. The difference between the literature data and the used values is due to the symmetric phase-diagram, which is used instead of the real phase-diagram of the alloy.

Parameter	literature data	value used
D (diffusion coefficient)	0.5 $\times 10^{-9}$ m^2/s	0.5 $\times 10^{-9}$ m^2/s
v_p (pulling velocity)	1.5 μm/s	1.5 μm/s
G (thermal gradient)	110 K/cm	110 K/cm
k_α (partition coefficient)	0.75	1
k_β (partition coefficient)	1.5	1
m_α (liquid slope of α)	-82 K/mol	-164 K/mol
m_β (liquid slope of β)	164 K/mol	164 K/mol
$\bar{d}$ (average capillary length)	6.5 nm	6.5 nm
C_α (average capillary length)	8.8 mol%	8.8 mol%
C_β (average capillary length)	18.5 mol%	18.5 mol%
C_E (eutectic composition)	11.6 mol%	11.57 mol%
λ_{JH} (lamellar spacing)	6528.0 nm	6528.0 nm

where $\bar{\tau} = (\tau_\alpha + \tau_\beta)/2$. In the liquid phase $\tau(\vec{p}) = \bar{\tau}$. The elastic coupling constant, λ_e (Eq. 24), is fixed by $\lambda_e = \lambda_c$ so that $Y = X$. We scale lengths by W and time by $\bar{\tau}$. The scaled evolution equation becomes

$$\begin{aligned}\tilde{\tau}(p_i)\frac{\partial p_i}{\partial t} &= \nabla^2 p_i + \frac{2}{3}[-2p_i(1-p_i)(1-2p_i) + \sum_{j\neq i} p_j(1-p_j)(1-2p_j)] \\ &\quad +\lambda_c \sum_j \frac{\partial g_j}{\partial p_i}|_{\sum_i p_i=1}\left[(\mu A_j - B_j) - f_{el}^j\right] \quad \forall i,\end{aligned} \tag{47}$$

and

$$\frac{\partial \mu}{\partial t} = \vec{\nabla}.\left(\tilde{D}p_L\vec{\nabla}\mu - \vec{j}_{at}\right) - \sum_i A_i \frac{\partial g_i(\vec{p})}{\partial t} \quad \forall i. \tag{48}$$

The dimensionless parameters in the evolution equations are specified as

$$\tilde{\tau}(p_i) = \frac{\tau(\vec{p})}{\bar{\tau}}, \quad \tilde{D} = \frac{D\bar{\tau}}{W^2}. \tag{49}$$

The coefficients A_i and B_i can be approximated by linearising the phase-diagram around the eutectic point, considering the fact that the front temperature is close to T_E in coupled eutectic growth at low solidification speeds [14]

$$\begin{aligned}A_i &= \frac{C_i - C_E}{\triangle C} + (k_i - 1)\frac{(\tilde{y} - \tilde{v}_p\bar{t})}{\bar{l}_T^i}, \\ B_i &= \mp A_i \frac{(\tilde{y} - \tilde{v}_p\bar{t})}{\bar{l}_T^i},\end{aligned} \tag{50}$$

Table 2: Parameters for symmetric alloy model computed from the data in Table 1 in the program codes for phase-field simulations.

Parameter	Value
λ_{JH}/W	64
$l_D/\bar{d}$	51200
$W/\bar{d}$	15.69
$\bar{l}_T/W$	10669
λ_c	18.098
$\tilde{D}$	5.3164
$\tilde{v}_p$	0.00199
$\triangle\tilde{t}$	0.0241

where $\tilde{y} = y/W$ and $\tilde{v}_p = v_p\bar{\tau}/W$. The minus (plus) sign corresponds to α (β) phase and k_i are partition coefficients, which are set to 1 (parallel liquidus and solidus lines). In this case, the initial composition of each phase are set to its equilibrium composition at the eutectic temperature.

3.2 Numerical Tests

The set of equations (47) and (48) are discretized by finite difference approach on a uniform mesh, while an explicit Euler scheme with a time step chosen below the stability limits of diffusion equation is used for time discretization.

$$\triangle t < \frac{1}{4\tilde{D}}(\triangle x)^2 \tag{51}$$

All program codes are written in C++ language, while Matlab is used for post-processing.

Table 3: Elasticity parameters used in simulations; the Lame constants are estimated values.

Parameter	Value used
$\lambda_e = \lambda_c$	18.098
μ^α	34.24 MPa
μ^β	32.2 MPa
λ^α	8.58 MPa
λ^β	7.8 MPa
$Y = X$	18.10 MPa

Starting from initial conditions for phase-field variables, chemical potential μ, and elastic displacements, the mechanical equilibrium equations Eq. 30-31 and the diffusion equation Eq. 21, should be solved independently. Once the chemical potential and displacements are computed, the driving forces of the phase transformation will be calculated. The new values

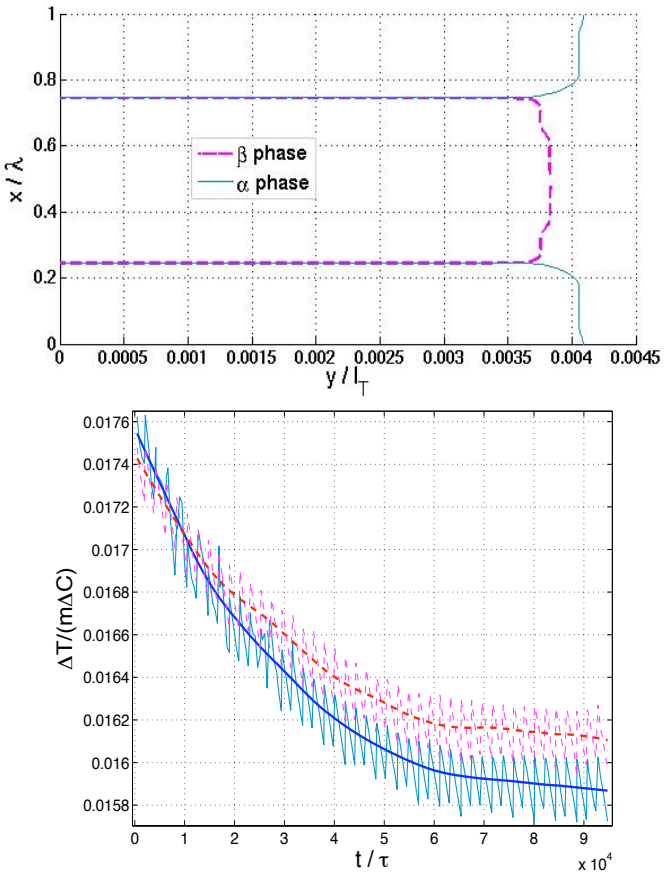

Figure 1: Front position of α and β lamellae (a) and the average front undercooling converging to steady state (b). Solid lines, α phase; dashed lines, β phase.

of driving forces will be inserted in the phase-field solver the phase-field variables will be updated. This procedure should be repeated in each time step.

The two dimensional simulations are performed in a rectangular box with symmetric boundary conditions in $y-$directions and no-flux boundary conditions in $x-$directions, applied to both phase-filed variables and concentration field. We use the grid spacing $\triangle x/W = 0.8$, the parameters $\bar{l}_T/l_D = 4$ and $l_D/\bar{d} = 51200$ in most of the simulations. All material and simulation parameters used are listed in Tables (1) and (2) respectively.

We first perform a series of simulations for a symmetric phase diagram, in which $|m_\alpha| = |m_\beta| = m$. The inhomogeneous isotropic elasticity, in which β phase is assumed to be softer, i.e $\mu_\beta(\lambda_\beta) < \mu_\alpha(\lambda_\alpha)$, is considered here. The elastic parameters are given in Table (3). The mechanical equilibrium equations are solved independently by applying UMFPACK solver [28]. The displacement fields are set to zero at the beginning of the simulations and have a zero value at the end of the simulation box. Symmetric boundary conditions is applied to displacement fileds in $y-$directions. The simulations start with lamellar of both phases with equal spacing and flat front. The size of the simulation box in $y-$direction is chosen about 5 times larger than its size along $x-$direction. In each time step we first solve the mechanical equilibrium and compute the corresponding displacement fields u_x and u_y along x any y directions, and three strain fields u_{xx}, u_{yy}, u_{xy} from Eq. (**??**). Once the strain fields are computed we insert their values in the phase-field equations and update the evolutionary

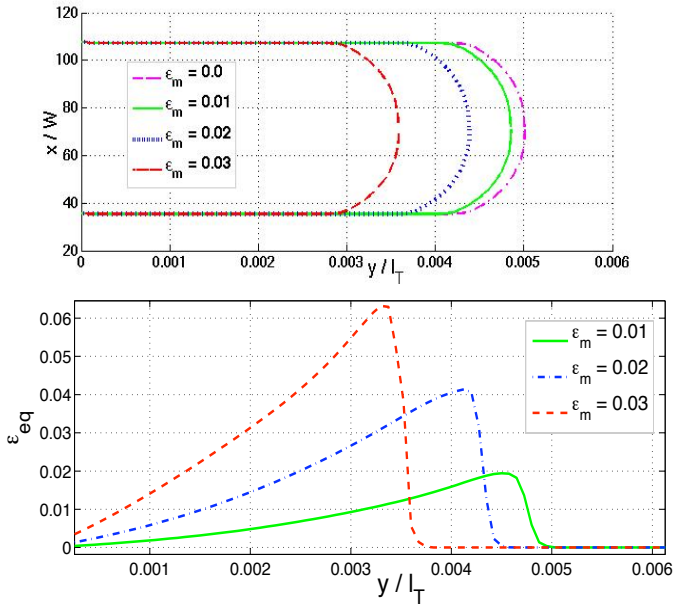

Figure 2: Influence of the misfit strain on eutectic growth: steady state configuration of β phase (a) the corresponding value of equivalent strain field, i.e $\sqrt{\epsilon_{xx}^2 + \epsilon_{yy}^2 + 2\epsilon_{xy}^2}$,(b).

equation.

In Fig. 1(a) the lamellae of α and β with spacing λ are illustrated, where a misfit strain $\epsilon_m = 0.015$ is applied to both phases. One can see that the β phase is suppressed and grows with a slower rate compared with α phase. The y position of the solid-liquid interface, averaged over x, and hence the front undercooling, $\triangle T/m\triangle C$, in the β phase is smaller than in the α phase, Fig. 1(b). Since in the symmetric alloy phase-diagram we assumed equal liquid slope m for both phases, this difference can be understood only as the influence of the elastic energy which is smaller for β phase. We now investigate the influence of misfit strain on the lamellar growth by comparing the y position of β phase for three runs with different values of ϵ_m after the same simulation time. Fig. 2(a) shows that as ϵ_m has decreased the front undercooling has reduced, therefore the β phase with the largest misfit has the most advanced front. The value of equivalent strain, which we define it as $\sqrt{\epsilon_{xx}^2 + \epsilon_{yy}^2 + 2\epsilon_{xy}^2}$, plotted in front of β phase along $y-$direction has increased with ϵ_m, Fig. 2(b). In Fig. 3, we show the configuration of three components of the stress tensor as well as the α and β phases plotted across the $x-$direction. As a semi-quantitative test for our phase-field model, we perform a series of simulations with fixed physical and material parameters by varying the lateral size of the simulation box, and hence changing the lamellar spacing λ, and considering the dependance of the dimensionless front undercooling, $\triangle\overline{T}$, versus lamellar spacing. In directional solidification of regular eutectic alloys the system selects the lamellar spacing giving a minimum front undercooling at the point denoted by λ_m [8]. This is the so-called Jackson-Hunt lamellar spasing λ_{JH} [27].

The average front undercooling in the simulation is defined as

$$\frac{\triangle T}{m\triangle C} = \frac{1}{L}\int_0^L y(x,t)dx - v_p t, \tag{52}$$

where L is the lateral box size and $y(x,t)$ is the y position of the front interface at time t.

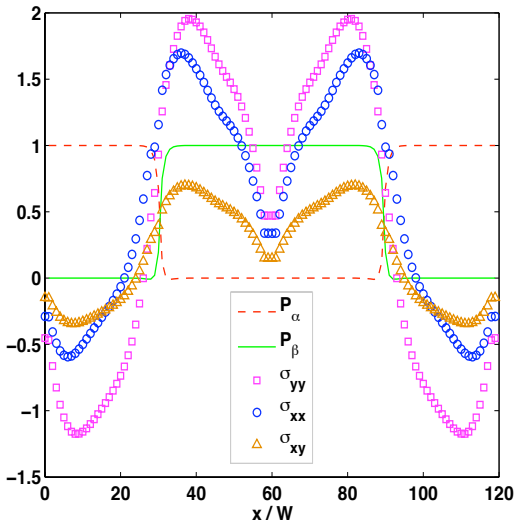

Figure 3: Components of the dimensionless stress tensor in α and β phases, $\bar{\sigma}_{ij} = (10\sigma_{ij})/Y$ with $i, j = x, y$.

Each run should reach the steady state. This has been achieved by shifting the simulation box periodically in growth direction with the pulling velocity and checking the change of the front undercooling by extracting the interface position until $\triangle T$ converges to a steady state value. In the simulations we have investigated the effects of misfit strain in phase-field model by comparing the Jackson-Hunt curve for our model with the case of diffusion limited two-phase growth without elastic effects similar to Ref. [14]. The symmetric alloy model with the same physical and model parameters as in Tables 1, 2 and 3 is used here. Moreover we assume $\mu_\alpha(\lambda_\alpha) = \mu_\beta(\lambda_\beta)$. The results for an elastic problem with different $\epsilon_m = 0.005, 0.01, 0.015$ are plotted in Fig. 4 in comparison with the same model without elastic effects ($\epsilon_m = 0$). It is obvious that the undercooling increases with increasing elastic field, because the driving force of solidification decrease with increasing elastic energy according to the elastic phase-field model. In Fig. 4 can be seen that the extreme value of λ_m increases with increasing ϵ_m too. This is due to weakening the elastic effects at larger lamellar spacing, because the misfit strain is present only near the interface between two phases (see Fig. 3). This means also that in the presence of misfit strain the lamellar are stable in larger spacing.

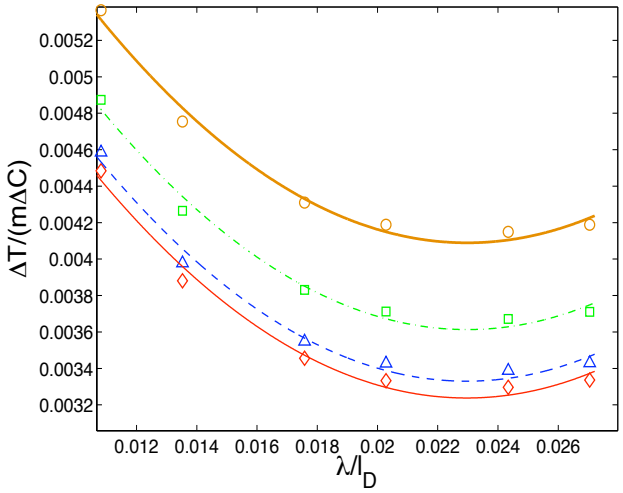

Figure 4: Dimensionless front undercooling versus dimensionless lamellar spacing for the model without elastic effects and with different misfit strains. Thin solid line, a quadratic fit to data obtained without considering elastic effects; dotted lines, ϵ_m=0.01; dashed dotted line, ϵ_m=0.02; thick solid line, ϵ_m=0.03.

4 Conclusions

The phase-field model of eutectic alloys is extended to take into account the influence of elastic interactions between lamellae of different phases. The elastic deformations and the corresponding stress distributions in lamellar eutectics are evaluated by solving the governing model equations, which include the coupling relations among phase-field variables, concentration and stress/strain fields. The microelastcity theory employed here is based on linear elasticity; however it allows to use inhomogenous elasticity with different elastic constants in solid phases. Furthermore we show that for each solid-liquid interface the evolutionary equations with elastic effects can be mapped to single-phase solidification.

The elastic effects caused by lattice misfit between two solid phases were investigated by plotting the undercooling of front interface versus lamellar spacing. We found that the extreme value of the lamellar spacing is larger for the problem including coherent misfit compared with pure diffusion limited eutectic growth. Therefore the lamellar are more stabilized by incorporating the elastic energy in to the model. Although we have tested our model for a symmetric eutectic model, it is capable to accommodate an arbitrary eutectic phase diagram and can be used to model the solidification of real eutectic systems e.g Ti-based alloys that exhibit a high elastic strain at the interfaces between the β-Ti (A2) and the non-stoichiometric FeTi(B2) phase, based on experimental observations [19, 20].

The presented phase-field model can also be applied to the larger lamellar arrays to predict the kinetics of eutectic front, e.g. wavelength selection and interface instabilities, under elastic interactions.

Acknowledgments

Financial support from the Deutsche Forschungsgemeinschaft (German Research Association) through grant GSC 111 is gratefully acknowledged.

References

[1] W.J. Boettinger, and G. B. McFadden, Phys. Rev. E 1992; **45**: 7424.

[2] S.G.Kim, W.T. Kim, T.Suzuki, Phys. Rev. E 1999; **60** 7186.

[3] J. Das, K. B. Kim, W. Xu, W. Löser and J. Eckert, Mater. Sci. Eng. A 2007; **449**: 737.

[4] V. Datye and J.S. Langer, Phys. Rev. B 1981; **24**: 4155

[5] K. Kassner, C. Misbah, Phys. Rev. Lett. 1991; **66**: 1551

[6] R. Baumann, K. Kassner, C. Misbah, D. Temkin, Phys. Rev. Lett. 1995; **75**: 2445

[7] M. Ginibre, S. Akamatsu, and G. Faivre, Phys. Rev. E 1997; **56**: 780

[8] M. F. Zhu and C. P. Hong, Phys. Rev. B 2002; **66**: 155428

[9] W. Kurz and D.J. Fischer, Fundamentals of Influence of the misfit strain on eutectic growthsolidification, Trans Tech Publications, Aedermansdorf, (1986).

[10] I. Steinbach, F.Pezzolla, B. Nestler, J. Rezende, M. Seesselberg and G. J. Schmitz, Physica D 1996; **94**: 135.

[11] J. Tiaden, B. Nestler, H.J. Diepers, and I. Steinbach, Physica D 1998; **115**: 73.

[12] B. Nestler and A. A. Wheeler, Physica D 2000; **138**: 114

[13] J. Eiken, B. Boettger, and I. Steinbach, Phys. Rev. E 2006; **73**: 066122.

[14] R. Folch and M. Plapp, Phys. Rev. E 2005; **72**: 011602

[15] J. Kundin, R. Siquieri, Submitted to Physica D 2010.

[16] P. Fratzl, O. Penrose, and J. L. Lebowitz, J. Stat. Phys. 1999; **95**:1429.

[17] I. Steinbach and M. Apel, Acta. Mater. 2007; **55**: 4817

[18] M. Fleck, C. Hüter, D. Pilipenko, R. Spatschek and E. A. Brener, Philosophical Magazine 2009;

[19] J. Das, K. B. Kim, F. Baier, W. Löser and J. Eckert, Appl. Phys. Lett. 2005; **87**: 161907

[20] R. Phillips: Crystals, Defects and Microstructures: Modeling Across Scales, Cambridge University Press, (2001).

[21] A. G. Khachaturyan, Theory of structural transformations in solids, Wiley, New York, (1983).

[22] A. Artemev, Y. Wang and A. G. Khachaturyan, Acta. Mater. 2000; **48**: 2503

[23] H. Emmerich, Continuum Mech. Thermodyn. 2003; **15**: 197.

[24] B. Echebarria, R. Folch, A. Karma, and M. Plapp, Phys. Rev. E 2004; **70**: 061604

[25] M. Plapp and A. Karma, Phys. Rev. E 2002; **66**: 061608

[26] A. Karma and W. J. Rappel, Phys. Rev. E 1998; **57**: 4

[27] K. A. Jackson and J. D. Hunt, Trans. Metall. Soc. AIME 1966; **236**: 843

[28] UMFPACK Version 5.2, Copyright (c) 1995-2009 by Timothy A. Davis, University of Florida. http://www.cise.ufl.edu/research/sparse/umfpack

List of Figures

List of Tables